RSC Advances

ROYAL SOCIETY OF CHEMISTRY

www.rsc.org/advances

New (1-x)$K_{0.5}Na_{0.5}NbO_3$–x(0.15$Bi_{0.5}Na_{0.5}TiO_3$–0.85$Bi_{0.5}Na_{0.5}ZrO_3$) ternary lead-free ceramics: microstructure and electrical properties

Qian Gou, Ding-Quan Xiao[a)], Bo Wu, Min Xiao, Sha-Sha Feng, Dan-Dan Ma Zhao, Jia-Gang Wu, and Jian-Guo Zhu

Department of Materials Science, Sichuan University, Chengdu 610064, P. R. China

Submitted to

RSC Advances

a) Author to whom correspondence should be addressed: Tel and Fax: 86-28-85412202
E-mail: nic0402@scu.edu.cn; Tel: +86-28-85412415; Fax: +86-28-85416050

Abstract

Lead-free piezoelectric ceramics have attracted considerable attention owing to their environmental friendliness and good electrical properties. Here the new (1-x)$K_{0.5}Na_{0.5}NbO_3$–x($0.15Bi_{0.5}Na_{0.5}TiO_3$–$0.85Bi_{0.5}Na_{0.5}ZrO_3$) [(1-$x$)KNN–$x$(BNT–BNZ)] ternary lead-free piezoelectric ceramics synthesized by conventional solid sintering method were reported. The microstructure and electrical properties of (1-x)KNN–x(BNT–BNZ) ternary ceramics were systematically investigated, and the ceramics with x=0.06 possess the enhanced piezoelectric properties and a high T_C (e.g., d_{33}~318 pC/N, k_p~0.43, and T_C~326°C), which are mainly ascribed to the involved R-T phase boundary. It is believed that, such a ceramic system is one of the promising candidates in the field of lead-free piezoelectric ceramics.

Keywords: Lead-Free Piezoelectric Ceramic; Piezoelectric Properties; Phase Boundary; Microstructure

1. Introduction

Lead zirconate titanate (PZT)-based piezoelectric materials are widely used in sensors, actuators and other electronic devices, owing to their excellent piezoelectric properties and a high Curie temperature (T_C).[1-3] However, the lead is harmful to the environment and human health. Therefore, it is a tough issue with great significance to develop lead-free piezoelectric materials for the replacement of these lead-based ceramics.[4-13]

In the past decades, several kinds of lead-free piezoelectric ceramics with perovskite structure, such as $BaTiO_3$ (BT), $(Bi_{0.5}Na_{0.5})TiO_3$ (BNT), and $(K,Na)NbO_3$ (KNN) ceramics, have been studied. BT is the first practically used piezoelectric ceramics. However, the poor piezoelectric properties and low Curie temperature of BT ceramics greatly limit their wider commercial application. Extensive efforts have been carried out to improve the piezoelectric properties and temperature stability of BT ceramics.[14-19] BNT is an important lead-free piezoelectric material, but BNT often exhibits poor piezoelectric properties. In order to improve the piezoelectric properties of BNT, a series of BNT-based lead-free piezoelectric ceramics with another perovskite components and the doping with other oxides were widely investigated.[20-24] Among those, the KNN-based ceramics are considered as the most promising candidates to replace lead-based ceramics because of their relatively excellent piezoelectric properties and high T_C.[5, 7-9, 11-13, 25-32]

Recently, it was reported that a small amount of $Bi_{0.5}Na_{0.5}TiO_3$ (BNT) was used to improve the sintering behavior and piezoelectric properties of KNN-based ceramics.[33] Nevertheless, these systems also show a poor piezoelectric activity. On the other hand, previous studies in the Authors' group have confirmed that the piezoelectric and

ferroelectric properties of KNN-based ceramics could remarkably be improved by adding $Bi_{0.5}Na_{0.5}ZrO_3$ (BNZ),[34] and the Authors' group invented a series of KNN–$(Bi,Na)(Zr,Ti)O_3$ (KNN–BNZT) and KNN–$[Bi,(K/Li)(Zr,Ti)]O_3$ (KNN–BK/LZT)-based lead-free piezoceramics very recently.[35-36] However, there were few reports on the microstructure and electrical properties of KNN–BNT–BNZ ternary lead-free ceramics in detail.

In this work, $(1-x)K_{0.5}Na_{0.5}Nb$–$x(0.15Bi_{0.5}Na_{0.5}TiO_3$–$0.85Bi_{0.5}Na_{0.5}ZrO_3)$ [(1-*x*)KNN–*x*(BNT–BNZ)] ternary ceramics were prepared by the conventional solid reaction method, the effects of BNT-BNZ content on the microstructure and electrical properties of (1-*x*)KNN–*x*(BNT–BNZ) ternary ceramics were systematically investigated, and some related physical mechanisms were studied.

2. Experimental procedure

(1-*x*)KNN–*x*(BNT–BNZ) ternary ceramics with *x*=0, 0.01, 0.02, 0.03, 0.04, 0.05, 0.06, and 0.07 were prepared by the conventional solid-state reaction route. Raw materials were K_2CO_3 (99.0%), Na_2CO_3 (99.8%), Nb_2O_5 (99.5%), Bi_2O_3 (99.0%), ZrO_2 (99%), and TiO_2 (99%) respectively. Raw powders were thoroughly mixed with ZrO_2 balls for 24 h using ethanol as the medium, and then dried and calcined at 850°C for 6 h. Calcined powders were mixed with a poly vinyl alcohol (PVA) binder solution and compacted into disk samples with a diameter of ~1.0 cm and a thickness of ~1.0 mm. Those samples were sintered in air at the temperature of 1070~1130°C for 3 h after burning out the PVA binder at 850°C for 2 h. Silver pastes were fired at 700°C for 10 min on both sides of these samples as electrodes

for electrical measurements. All samples were poled at room temperature in a silicone oil bath under a dc field of 4.0 kV/mm for 20 min.

The phase structure of these sintered samples was measured using X-ray diffraction (XRD) (Bruker D8 Advanced XRD, Bruker AXS Inc, Madison, WI, CuKα). The surface morphology of these sintered samples was analyzed by the field emission-scanning electron microscopy (FE-SEM) (JSP 7500, Japan). The temperature dependence dielectric behavior of these sintered samples was characterized using a programmable furnace with an *LCR* analyzer (HP 4980, Agilent, U.S.A.). The d_{33} of the samples was tested using a piezo-d_{33} meter (ZJ-3A, China), the dielectric properties of the samples were measured using an impedance analyzer (HP 4294A), and the hysteresis loops of the samples were characterized using a Radiant Precision Workstation (USA).

3. Results and discussion

Fig. 1(a) shows the XRD patterns of the ceramics as a function of BNT–BNZ content in the 2θ range of 20~60°. All ceramics are of a pure perovskite phase, and no secondary phases are observed in the composition range investigated, confirming that the stable solid solutions between KNN and BNT–BNZ are formed in this work. Their correspondingly expanded XRD patterns in the 2θ range of 44~47° are represented in Fig. 1(b). A small amount of BNT–BNZ can not change the crystal structure of KNN ceramics, that is to say, an orthorhombic phase is still observed in the ceramics with $x \leq 0.02$. With the increase of BNT–BNZ content, an orthorhombic-tetragonal (O–T) phase coexistence is found in the ceramics with $0.03 \leq x \leq 0.04$. For the ceramics with $x=0.07$, the rhombohedral-tetragonal (R–T)

phase is suppressed. So we can confirm that the R–T phase coexistence has been existed in the ceramics with $0.05 \leq x < 0.07$.

To further indicate the variation of phase structures, the temperature dependence of the dielectric constant (ε_r) of (1-x)KNN–x(BNT–BNZ) ternary ceramics was measured in the temperature range of -150~200°C, as illustrated in Fig. 2. As represented in Fig. 2(a~e), the T_{R-O} peaks can be clearly observed for the ceramics with x=0~0.04, increasing with the increase of BNT–BNZ content, while the T_{O-T} peaks are gradually shifted to a lower temperature with rising BNT–BNZ content. The T_{R-O} and T_{O-T} peaks gradually develop into a single one as the BNT–BNZ further increases, as shown in Fig. 2(f) and (g). Such a result shows that T_{R-O} and T_{O-T} peaks get together, and the T_{R-T} peaks appear when the BNT–BNZ content raises up to 0.05. However, with continually increasing x (=0.07), the T_{R-T} peaks evolve to be much more broadened and even disappear because of the dramatic decreased grain size [see fig. 5(d)], indicating that the R–T phase boundary has been suppressed.[37-38]

As shown in Fig. 3(a), the ceramics with x=0~0.04 possess two dielectric peaks above room temperature, which are assigned to orthorhombic to tetragonal phase temperature (T_{O-T}) and tetragonal to cubic phase temperature (T_C), while only one dielectric peak (T_C) is observed in the ceramics with x=0.05~0.07. It can be found from Fig. 3(b) that the T_C of those ceramics generally decreases with the rise of BNT–BNZ content, and the composition with x=0.06 shows a relatively high T_C of 326°C, which is much higher than other KNN-based ceramics.[39-42] As illustrated in Fig. 3(c), the T_{O-T} of the ceramics with x=0~0.04 decreases with increasing BNT–BNZ content, which is consistent with the results of Fig. 2(a~e).

For further describing the phase transition of this work, the temperature-composition phase diagram of (1-x)KNN–x(BNT–BNZ) ternary ceramics has been identified by using the temperature dependence of dielectric constant[10, 43] in Fig. 2 and 3, as shown in Fig. 4. With the increase of BNT–BNZ content, the $T_{R\text{-}O}$ is gradually shifted to a higher temperature, and the T_C and $T_{O\text{-}T}$ have a decreasing trend. Both rhombohedral-orthorhombic and orthorhombic–tetragonal phase boundaries gradually move close to room temperature, and then the rhombohedral-tetragonal phase boundary can been seen in the ceramics with $0.05 \leq x < 0.07$. Considering the combination of XRD and the temperature dependence of dielectric constant, the phase coexistence of R–T can be confirmed in the compositional range of $0.05 \leq x < 0.07$.

Fig. 5(a)-(d) plot the SEM surface morphologies of the (1-x)KNN–x(BNT–BNZ) ternary ceramics as a function of BNT–BNZ content with x=0, 0.03, 0.06, and 0.07, respectively. The grain size of the ceramics increases sharply with rising BNT–BNZ content, reaching a maximum value at x=0.06, showing that a low concentration of BNT–BNZ has entered the lattice of KNN ceramics and promoted the grain growth. Nevertheless, with further increasing BNT–BNZ content, the grain size of the ceramics reduces dramatically because of the increasing of Bi^{3+}, which inhibits the grain growth.[44-45] The dramatic decreased grain size results in a more broadened T_{R-T} peak, and T_{R-T} peak even disappears, as shown in Fig. 2(h).

Fig. 6 shows the composition dependence of the piezoelectric constant (d_{33}) and electromechanical coupling factor (k_p) of (1-x)KNN–x(BNT–BNZ) ternary ceramics, where all samples were poled and measured at room temperature. The d_{33} values of (1-x)KNN–x(BNT–BNZ) ternary ceramics raise with the increase of BNT–BNZ

content, reaches a maximum (d_{33}~318 pC/N) for the ceramic with x=0.06, and drastically reduces with further rising BNT–BNZ content. The k_p values show the similar change with rising BNT–BNZ content, and obtain a maximum (k_p~0.43) for the ceramics with x=0.06. The enhanced polarizability induced by the coupling between two equivalent energy states of the tetragonal and rhombohedral phases mainly results in large d_{33} and k_p values. The electrical domains in the R–T region have more possible polarization states and can rotate much easier by the external stresses and electric fields.

In this work, the ceramics with x=0.06 show a high d_{33} of 318 pC/N, which is much larger than those KNN-based ceramics.[33, 37, 42, 46] Furthermore, it is of great significance that the ceramics with x=0.06 also possess a higher T_C (326°C) than these KNN-based ceramics,[39-42] as shown in Table 1, and the higher T_C of the ceramics facilitates industrial applications in a wide temperature range.

Table. 1 Piezoelectric properties and Curie temperature of KNN-based ceramics

Materials system	d_{33}/(pC/N)	k_p	T_C /(°C)	Refs.
$(K_{0.4}Na_{0.52})(Nb_{0.84}Sb_{0.08})O_3$–$(0.08-x)LiTaO_3$–$xBaZrO_3$	365	0.45	178	Zuo[39]
$0.94(K_{0.4-x}Na_{0.6}Ba_xNb_{1-x}Zr_x)O_3$–$0.06LiSbO_3$	344	0.32	176	Liang[40]
$(K_{0.44-x} Na_{0.52})(Nb_{0.95-x}Sb_{0.05})O_3$–$xLiTaO_3$	321	0.52	315	Fu[41]
$(K_{0.55}Na_{0.45})_{0.965}Li_{0.035}Nb_{0.80}Ta_{0.20}O_3$	262	0.53	320	Zhang[42]
$(1-x)(K_{0.48}Na_{0.52})NbO_3$–$xBi_{0.5}(Na_{0.7}K_{0.2}Li_{0.1})_{0.5}ZrO_3$	236	0.38	350	Cheng[37]
$(1-x)K_{0.5}Na_{0.5}NbO_3$–$xBi_{0.5}Na_{0.5}TiO_3$	195	0.43	375	Zuo[33]

(1-x) $K_{0.5}Na_{0.5}NbO_3$–$xBi_{0.5}Li_{0.5}TiO_3$	172	0.37	381	Jiang[46]
(1-x)$K_{0.5}Na_{0.5}Nb$–x(0.15$Bi_{0.5}Na_{0.5}TiO_3$–0.85$Bi_{0.5}Na_{0.5}ZrO_3$)	318	0.43	326	This work

Fig. 7 displays the ε_r and tan δ values of (1-x)KNN–x(BNT–BNZ) ternary ceramics as a function of BNT-BNZ content, measured at room temperature. The ε_r values of (1-x)KNN–x(BNT–BNZ) ternary ceramics rise slightly with increasing BNT–BNZ content (x=0~0.03), then rise sharply in the range of 0.03<x<0.05, and almost maintain a constant at 0.05<x<0.07 due to R–T phase transition near room temperature. A lower tan δ value (tan δ=0.026) is demonstrated for the ceramics with x=0.06.

The P–E loops of the (1-x)KNN–x(BNT–BNZ) ternary ceramics as a function of BNT–BNZ content, measured in the frequency of 10 Hz at room temperature, are represented in Fig. 8(a). All the samples have typical ferroelectric P–E loops, especially for x=0.05~0.06, standing for their superior ferroelectric properties. To further display the composition dependence of their ferroelectric properties, the composition dependence of remanent polarization (P_r) and coercive field (E_c) is shown in Fig. 8(b). The P_r values significantly rise with increasing BNT-BNZ content, reach a maximum with x=0.05~0.06, and then drop dramatically due to the change of phase structure. The relatively large P_r values obtained by the samples with x=0.05 and 0.06 mainly originate from their unique R–T phase coexistence near room temperature, resulting in the instability of the polarization states, which can be easily rotated under the action of external electric fields. The E_c values reach maximum for the ceramics with x=0.06, and then drop as the x increases.

The generally used empirical formula of d_{33}~$\alpha\varepsilon_r P_r$ can be introduced to analyze the

new R–T structure and the effect of the dielectric and dipole properties on piezoelectric properties of the ceramics.[30, 34] Fig. 9 shows the d_{33} and $\varepsilon_r P_r$ values of (1-x)KNN–x(BNT–BNZ) ternary ceramics. The d_{33} and $\varepsilon_r P_r$ values of the ceramics have simultaneously reached peaks for the ceramics with the R–T phase boundaries, indicating that relatively high ε_r and P_r also play a role on the large d_{33}.

4. Conclusions

(1-x)$K_{0.5}Na_{0.5}Nb$–x(0.15$Bi_{0.5}Na_{0.5}TiO_3$–0.85$Bi_{0.5}Na_{0.5}ZrO_3$) [(1-x)KNN–x(BNT–BNZ)] ternary ceramics were prepared by the conventional solid reaction method. The suitable amount of BNT–BNZ to KNN greatly improves the piezoelectric and ferroelectric properties. The ceramics with x=0.06 possess enhanced electrical properties and a high T_C: d_{33}~318 pC/N, k_p~0.43, ε_r~1604, tan δ~0.026, P_r~16.8 μC/cm^2, E_c~12.3 kV/cm, and T_C~326°C, which are mainly ascribed to the involved R–T phase boundary. As result, the material system is a promising candidate for lead-free piezoelectric applications in the near future.

Acknowledgements

This work was supported by National Science Foundation of China (NSFC Nos.50772068, 50972095, 51272164, and 51332003). Thanks are also to Ms Wang Hui for her help in the SEM measurement.

References

1. B. Jaffe, W. R. Cook, and H. Jaffe, *"Piezoelectric Ceramics"*, Academic Press, New York, 1971.
2. R. E. Newnham, S. K. Majumdar, R. E. Tressler, and E. W. Miller, "*Functional Composites for Sensors and Actuators: Smart Materials"*, The Pennsylvania Academy of Science, Pennsylvania, 1998.
3. K. Uchino, *"Piezoelectric Actuators and Ultrasonic Motors"*, Kluwer Academic Publishers, Boston, 1997.
4. L. E. Cross, "Lead Free at Last", *Nature*, 432 (2004), pp. 24-25.
5. Y. Saito, H. Takao, T. Tani, T. Nonoyama, K. Takatori, T. Homma, T. Nagaya, and M. Nakamura, "Lead-Free Piezoceramics*", Nature*, 432 (2004), pp. 84-87.
6. T. Takenaka, and H. Nagata, "Current Status and Prospects of Lead-Free Piezoelectric Ceramics", *J. Eur. Ceram. Soc.*, 25 (2005), pp. 2693-2700.
7. T. R. Shrout, and S. J. Zhang, "Lead-Free Piezoelectric Ceramics: Alternatives for PZT" *J. Electroceram.*, 19 (2007), pp. 113-126.
8. J. Rödel, W. Jo, K. T. P. Seifert, E. M. Anton, T. Granzow, and D. Damjanovic, "Perspective on the Development of Lead-Free Piezoceramics", *J. Am. Ceram. Soc*., 92 (2009), pp. 1153-1177.
9. P. K. Panda, "Review: Environmental Friendly Lead-Free Piezoelectric Materials", *J. Mater. Sci*., 44 (2009), pp. 5049-5062.
10. W. F. Liu, and X. B. Ren, "Large Piezoelectric Effect in Pb-Free Ceramics", *Phys. Rev. Lett*., 103 (2009), pp. 257602.
11. D. Q. Xiao, J. G. Wu, L. Wu, J. G. Zhu, P. Yu, D. M. Lin, Y. W. Liao, and Y. Sun, "Investigation on the Composition Design and Properties Study of Perovskite Lead-Free Piezoelectric Ceramics", *J. Mater. Sci*., 44 (2009), pp.

5408-5419.

12. W. Jo, R. Dittmer, M. Acosta, J. Zang, C. Groh, E. Sapper, K. Wang, and J. Rödel, "Giant Electric-Field-Induced Strains in Lead-Free Ceramics for Actuator Applications-Status and Perspective", *J. Electroceram*., 29 (2012) , pp. 71-93.
13. M. Matsubara, T. Yamaguchi, W. Sakamoto, K. Kikuta, T. Yogo, and S. Hirano, "Processing and Piezoelectric Properties of Lead-Free (K,Na)(Nb,Ta)O_3 Ceramics", *J. Am. Ceram. Soc*., 88 (2005), pp.1190-1196.
14. P. Zheng, J. L. Zhang, S. F. Shao, Y. Q. Tan, and C. L. Wang, "Piezoelectric Properties and Stabilities of CuO-Modified Ba(Ti,Zr)O_3 Ceramics", *Appl. Phys. Lett.*, 94 (2009), pp. 032902.
15. H. Y. Guo, C. Lei, and Z. G. Ye, "Reentrant Type Relaxor Behavior in(1-*x*)$BaTiO_3$–*x*$BiScO_3$ Solid Solution", *Appl. Phys. Lett.*, 92 (2008), pp. 172901.
16. B. Xiong, H. Hao, S. Zhang, H. Liu, and M. Cao, "Structure, Dielectric Properties and Temperature Stability of $BaTiO_3$–$Bi(Mg_{1/2}Ti_{1/2})O_3$ Perovskite Solid Solutions", *J. Am. Ceram. Soc.*, 94 (2011), pp. 3412–3417.
17. F. Benabdallah1, A. Simon, H. Khemakhem, C. Elissalde, and M. Maglione, "Linking Large Piezoelectric Coefficients to Highly Flexible Polarization of Lead Free $BaTiO_3$–$CaTiO_3$–$BaZrO_3$ Ceramics", *J. Appl. Phys.*, 109 (2011), pp. 124116.
18. L. Dong, D. S. Stone, and R. S. Lakes, "Enhanced Dielectric and Piezoelectric Properties of *x*$BaZrO_3$–(1-*x*)$BaTiO_3$ ceramics", *J. Appl. Phys.*, 111 (2012), pp. 084107.
19. D. Z. Xue, Y. M. Zhou, H. X. Bao, J. H. Gao, C. Zhou, and X. B. Ren, "Large

Piezoelectric Effect in Pb-Free $Ba(Ti,Sn)O_3$–$x(Ba,Ca)TiO_3$ Ceramics", *Appl. Phys. Lett.*, 99 (2011), pp. 122901.

20. K. Yoshii, Y. Hiruma, H. Nagata, and T. Takenaka, "Electrical Properties and Depolarization Temperature of $(Bi_{1/2}Na_{1/2})TiO_3$–$(Bi_{1/2}K_{1/2})TiO_3$ Lead-Free Piezoelectric Ceramics", *Jpn. J. Appl. Phys.*, 45 (2006), pp. 4493.
21. G. F. Fan, W. Z. Lu, X . H. Wang, and F. Liang, "Morphotropic Phase Boundary and Piezoelectric Properties of $(Bi_{1/2}Na_{1/2})TiO_3$–$(Bi_{1/2}K_{1/2})TiO_3$–$KNbO_3$ Lead-Free Piezoelectric Ceramics", *Appl. Phys. Lett.*, 91 (2007), pp. 202908.
22. S. T. Zhang, F. Yan, B. Yang, and W. W. Cao, "Phase Diagram and Electrostrictive Properties of $Bi_{0.5}Na_{0.5}TiO_3$–$BaTiO_3$–$K_{0.5}Na_{0.5}NbO_3$ Ceramics", *Appl. Phys. Lett.*, 97 (2010), pp. 122901.
23. M. K. Zhu, L. Y. Liu, Y. D. Hou, H. Wang, and H. Yan, "Microstructure and Electrical Properties of MnO-Doped $(Na_{0.5}Bi_{0.5})_{0.92}Ba_{0.08}TiO_3$ Lead-Free Piezoceramics", *J. Am. Ceram. Soc.*, 90 (2007), pp. 120-124.
24. T. S. Zhou, R. X. Huang, X. Z. Shang, F. Peng, J. Y. Guo, L. Y. Chai, H. S. Gu, and Y. B. He, "Lead-free In_2O_3-Doped $(Bi_{0.5}Na_{0.5})_{0.93}Ba_{0.07}TiO_3$ Ceramics Synthesized by Direct Reaction Sintering", *Appl. Phys. Lett.*, 90 (2007), pp. 182903.
25. J. F. Li, K. Wang, F. Y. Zhu, L. Q. Cheng, and F. Z. Yao, "$(K,Na)NbO_3$-Based Lead-Free Piezoceramics: Fundamental Aspects, Processing Technologies, and Remaining Challenges", *J. Am. Ceram. Soc.*, 96(2013), pp. 3677-3696.
26. S. J. Zhang, R. Xia, and T. R. Shrout, "Modified $(K_{0.5}Na_{0.5})NbO_3$ Based Lead-Free Piezoelectrics with Broad Temperature Usage Range", *Appl. Phys. Lett.*, 91 (2007), pp. 132913.

27. W. F. Liang, W. F .Wu, D. Q. Xiao, and J. G. Zhu, "Effect of the Addition of $CaZrO_3$ and $LiNbO_3$ on the Phase Transitions and Piezoelectric Properties of $K_{0.5}Na_{0.5}NbO_3$ Lead-Free Ceramics", *J. Am. Ceram. Soc.*, 94 (2009), pp. 4317-4322.

28. X. M. Pang, J. H. Qiu, and K. J. Zhu, "Morphotropic Phase Boundary of Sodium-Potassium Niobate Lead-Free Piezoelectric Ceramics", *J. Am. Ceram. Soc.*, 94 (2011), pp. 796-801.

29. X. P. Wang, J. G. Wu, D. Q. Xiao, J. G. Zhu, X. J. Cheng, T. Zheng, B. Y. Zhang, X. J. Lou, and X. J. Wang, "Giant Piezoelectricity in Potassium-Sodium Niobate Lead-Free Ceramics" , *J. Am. Chem. Soc*., 136 (2014), pp. 2905-2910.

30. H. Fu, and R. E. Cohen, "Polarization Rotation Mechanism for Ultrahigh Electromechanical Response in Single-Crystal Piezoelectrics", *Nature*, 403 (2000), pp. 281-283.

31. D. E. Cox, B. Noheda, G. Shirane, Y. Uesu, K. Fujishiro, and Y. Yamada, "Universal Phase Diagram for High-Piezoelectric Perovskite Systems", *Appl. Phys. Lett.*, 79 (2001), pp. 400-402.

32. X. J. Cheng, J. G. Wu, X. P. Wang, B. Y. Zhang, J. G. Zhu, D. Q. Xiao, X. J. Wang, and X. J. Lou, "Giant d_{33} in $(K,Na)(Nb,Sb)O_3$-$(Bi,Na,K,Li)ZrO_3$ Based Lead-Free Piezoelectrics with High T_c", *Appl. Phys. Lett.*, 103 (2013), pp. 052906.

33. R. Z. Zuo, X. S. Fang, and C. Ye, "Phase Structures and Electrical Properties of New Lead-Free $Na_{0.5}K_{0.5}NbO_3$–$Bi_{0.5}Na_{0.5}TiO_3$ Ceramics", *Appl. Phys. Lett*., 90 (2007), pp. 092904.

34. Z. Wang, D. Q. Xiao, J. G. Wu, M. Xiao, F. X. Li, and J. G. Zhu, "New Lead-Free $(1-x)(K_{0.5}Na_{0.5})NbO_3$-$x(Bi_{0.5}Na_{0.5})ZrO_3$ Ceramics with High

Piezoelectricity", *J. Am. Ceram . Soc*., 97 (2014), pp.688-690.

35. D. Q. Xiao, Z. Wang, M. Xiao, B. Wu, J. G. Wu, J. G. Zhu, and P. Yu, *Chinese Authorized Invention Patent*, ZL 201310200214.9., 2014-10-01.

36. D. Q. Xiao, Z. Wang, M. Xiao, B. Wu, J. G. Wu, J. G. Zhu, and P. Yu, *Chinese Authorized Invention Patent*, ZL 201310198923.8. 2014-10-01.

37. X. J. Cheng, Q. Gou, J. G. Wu, X. P. Wang, B. Y. Zhang, D. Q. Xiao, J. G. Zhu, X. J. Wang, and X. J. Lou, "Dielectric, Ferroelectric, and Piezoelectric Properties in Potassium Sodium Niobate Ceramics with Rhombohedral-Orthorhombic and Orthorhombic-Tetragonal Phase Boundaries", *Ceram. Int*., 40 (2014), pp. 5771-5779.

38. X. J. Cheng, J. G. Wu, T. Zheng, X. P. Wang, B. Y. Zhang, D. Q. Xiao, J. G. Zhu, X. J. Wang, and X. J. Lou, "Rhombohedral-Tetragonal Phase Coexistence and Piezoelectric Properties Based on Potassium-Sodium Niobate Ternary System", *J. Alloy. Compd.*, 610 (2014), pp. 86-91.

39. R. Z. Zuo, and J. Fu, "Rhombohedral-Tetragonal Phase Coexistence and Piezoelectric Properties of $(NaK)(NbSb)O_3$-$LiTaO_3$-$BaZrO_3$ Lead-Free Ceramics", *J. Am. Ceram. Soc.*, 94 (2011), pp. 1467-1470.

40. W. F. Liang, W. J. Wu, D. Q. Xiao, J. G. Zhu, and J. G. Wu, "Construction of New Morphotropic Phase Boundary in $0.94(K_{0.4-x}Na_{0.6}Ba_xNb_{1-x}Zr_x)O_3$–$0.06LiSbO_3$ Lead-Free Piezoelectric Ceramics". *Mater. Sci.*, 46 (2011), pp. 6871-6876.

41. J. Fu, R. Z. Zuo, D. Y. Lv, Y. Liu, and Y. Wu, "Structure and Piezoelectric Properties of Lead-Free $(Na_{0.52}K_{0.44-x})(Nb_{0.95-x}Sb_{0.05})O_3$–$xLiTaO_3$ Ceramics", *J. Mater. Sci.: Mater. Electron.*, 21 (2010), pp. 241-245.

42. J. L. Zhang, X. Zong, L. Wu, Y. Gao, P. Zheng, and S. F. Shao, "Polymorphic Phase Transition and Excellent Piezoelectric Performance of $(K_{0.55}Na_{0.45})_{0.965}Li_{0.035}Nb_{0.80}Ta_{0.20}O_3$ Lead-Free Ceramics", *Appl. Phys. Lett.*, 95 (2009), pp. 022909.

43. Y. G. Yao, C. Zhou, D. C. Lv, D. Wang, H. J. Wu, Y. D. Yang, and X. B. Ren, "Large Piezoelectricity and Dielectric Permittivity in $BaTiO_3$–$xBaSnO_3$ System: the Role of Phase Coexisting", *EPL*, 98 (2012), pp. 27008.

44. H. L. Du, W. C. Zhou, F. Luo, D. M. Zhu, S. B. Qu, and Z. B. Pei. "Perovskite Lithium and Bismuth Modified Potassium-Sodium Niobium Lead-Free Ceramics for High Temperature Applications", *J. Appl. Phys.,* 91 (2007), pp. 182909.

45. H. L. Du, W. C. Zhou, D. M. Zhu, and L. Fa. "Sintering Characteristic, Microstructure, and Dielectric Relaxor Behavior of $(K_{0.5}Na_{0.5})NbO_3$–$(Bi_{0.5}Na_{0.5})TiO_3$ Lead-Free Ceramics", *J. Am. Ceram. Soc.,* 91 (2008), pp.2903–2909.

46. X. P. Jiang, Q. Yang , Z. D. Yu , F. Hu, C. Chen, N. Tu, and Y. M. Li, "Microstructure and Electrical Properties of $Li_{0.5}Bi_{0.5}TiO_3$-Modified $(K_{0.5}Na_{0.5})NbO_3$ Lead-Free Piezoelectric Ceramics", *J. Alloys Compd.*, 493 (2010), pp. 276-280.

Figure Captions

Fig. 1 XRD patterns of the ceramics with different BNT–BNZ content: (a) 2θ=20~60°, (b) 2θ=44~47°.

Fig. 2 Temperature-dependence of the dielectric constant (ε_r) of (1-x)KNN–x(BNT–BNZ) ternary ceramics in the temperature from -150°C to 200°C: (a) x=0, (b) x=0.01, (c) x=0.02, (d) x=0.03, (e) x=0.04, (f) x=0.05, (g) x=0.06, and (h) x=0.07.

Fig. 3(a) ε_r–T (30~500°C) curves of (1-x)KNN–x(BNT–BNZ) (x=0~0.07) ternary ceramics, (b) the expanded ε_r-T (60~200°C) curves of (1-x)KNN–x(BNT–BNZ) (x=0~0.04) ternary ceramics, and (c) the T_C of the ceramics with different BNT–BNZ content.

Fig. 4 Phase diagram of (1-x)KNN–x(BNT–BNZ) ternary ceramics.

Fig. 5 SEM patterns of (1-x)KNN–x(BNT–BNZ) ternary ceramics as a function of BNT-BNZ content: (a) x=0, (b) x=0.03, (c) x=0.06, and (d) x=0.07.

Fig. 6 d_{33} and k_p values of (1-x)KNN–x(BNT–BNZ) ternary ceramics.

Fig. 7 ε_r and tan δ values of (1-x)KNN–x(BNT–BNZ) ternary ceramics.

Fig. 8 (a) P–E loops and (b) P_r and E_c values of (1-x)KNN–x(BNT–BNZ) ternary ceramics.

Fig. 9 d_{33} and $\varepsilon_r P_r$ values of (1-x)KNN–x(BNT–BNZ) ternary ceramics.

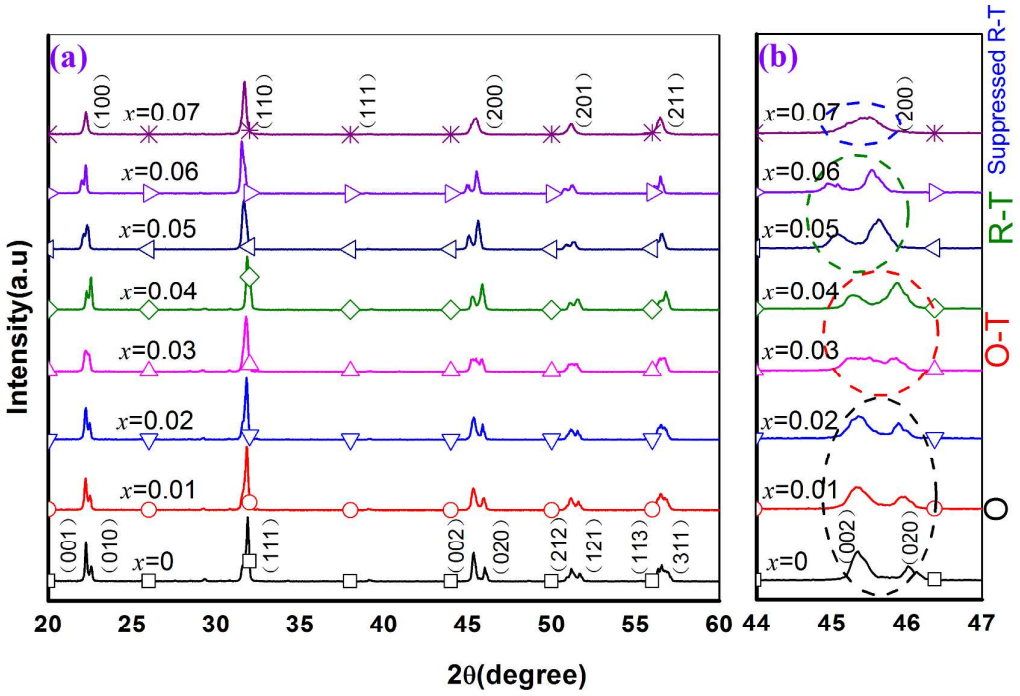

Fig.1

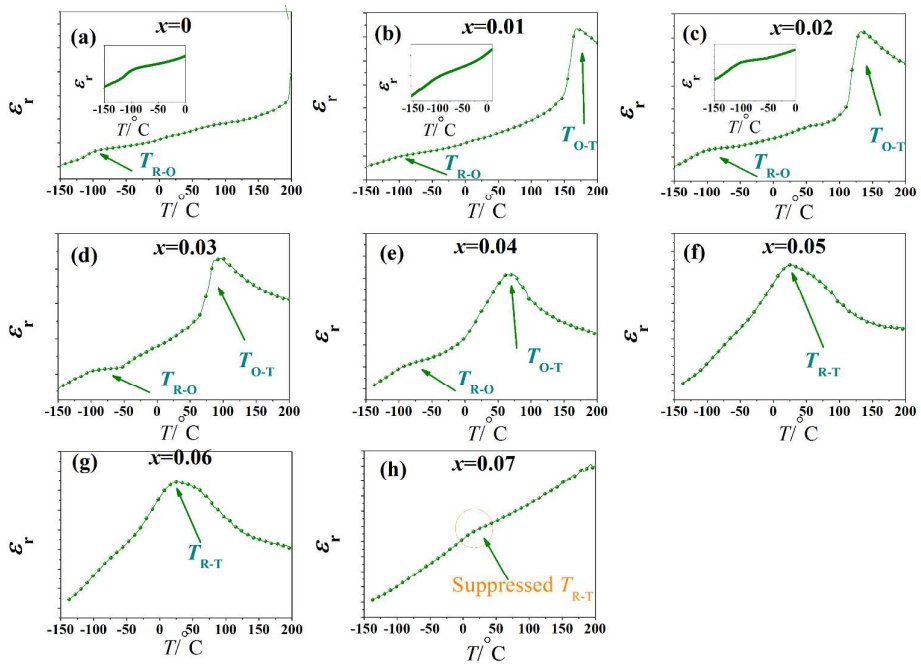

Fig. 2

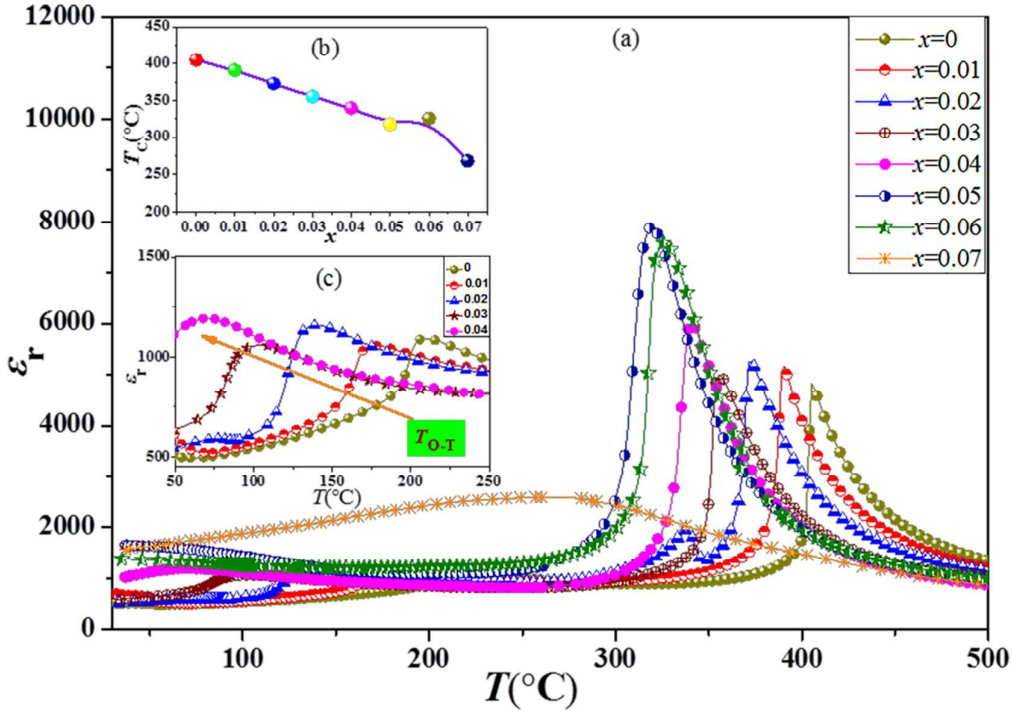

Fig. 3

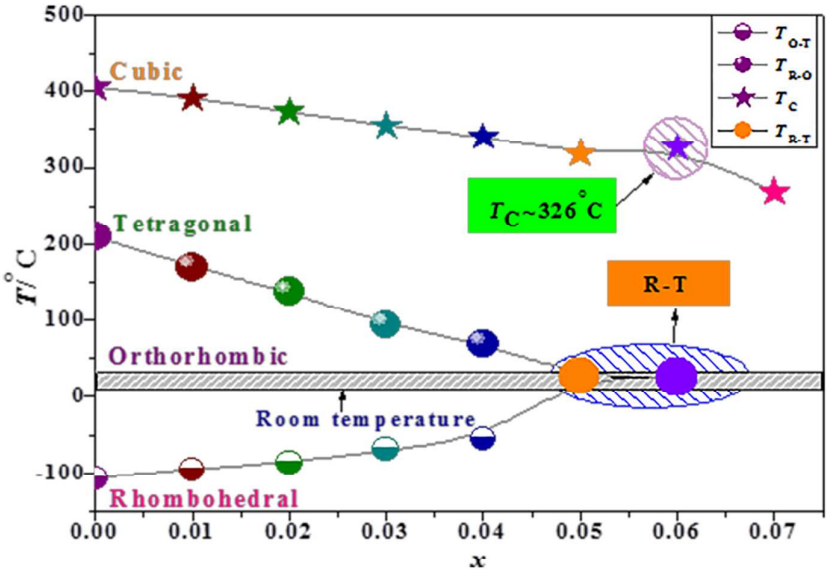

Fig. 4

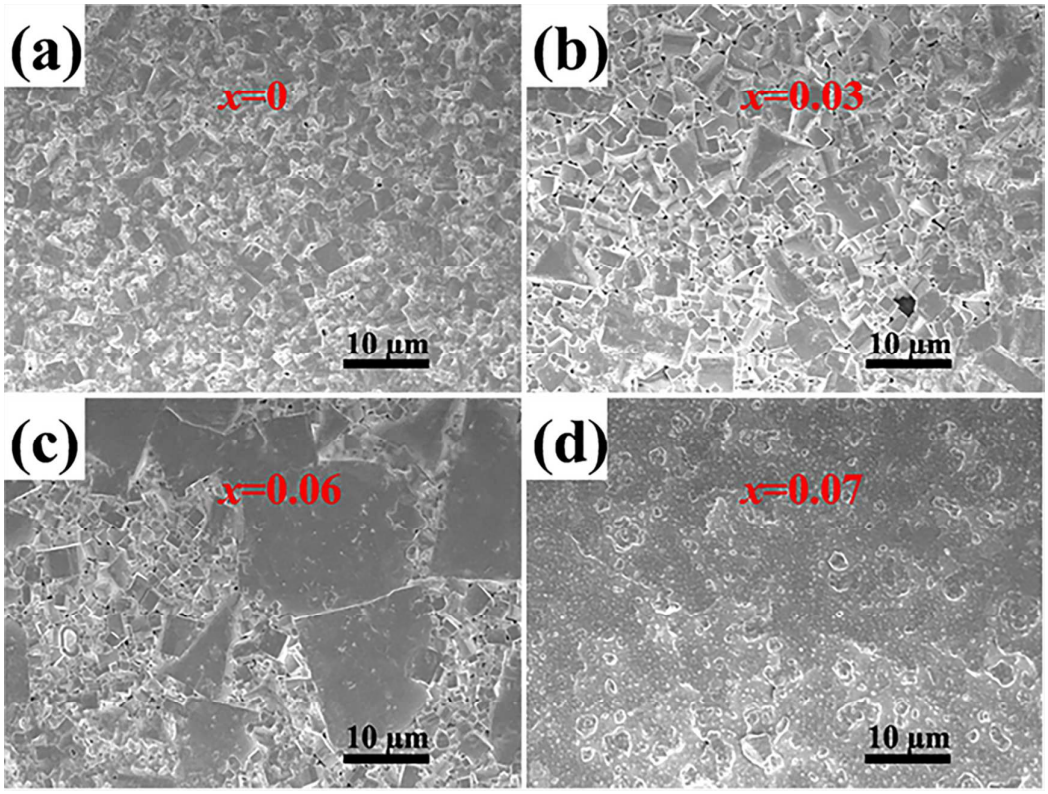

Fig. 5

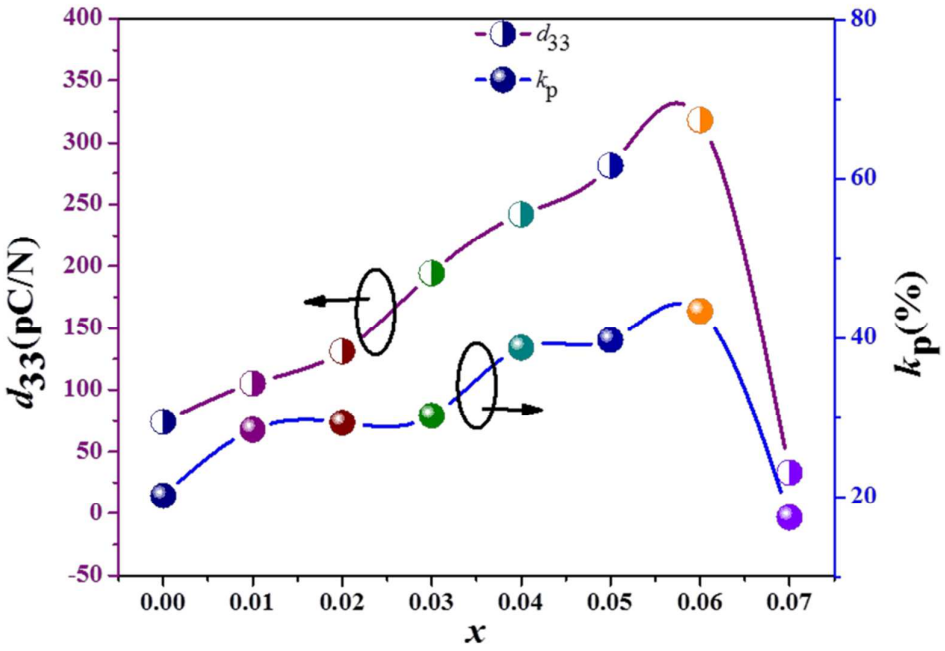

Fig. 6

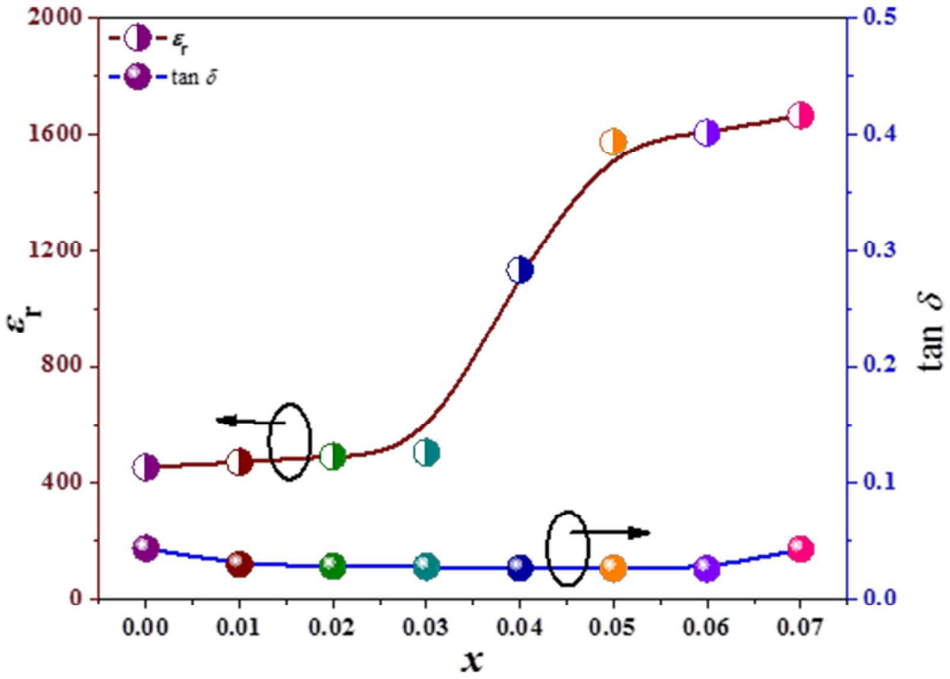

Fig.7

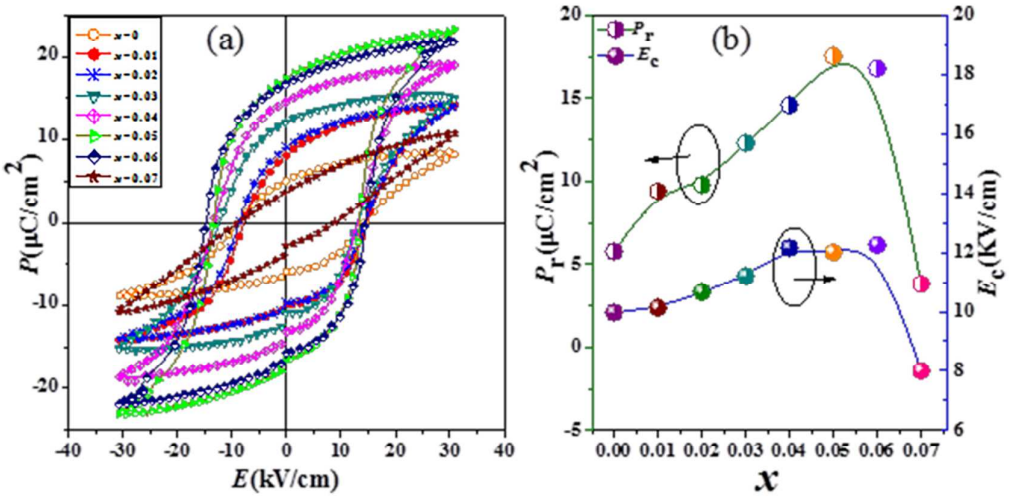

Fig. 8

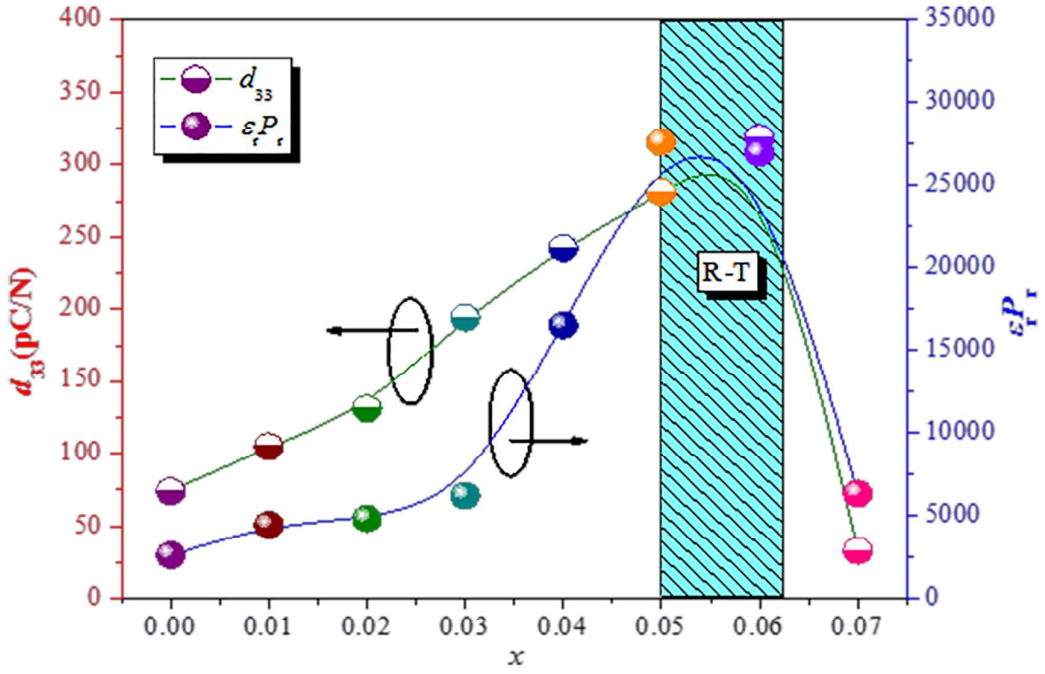

Fig. 9

Table of Contents Graphic

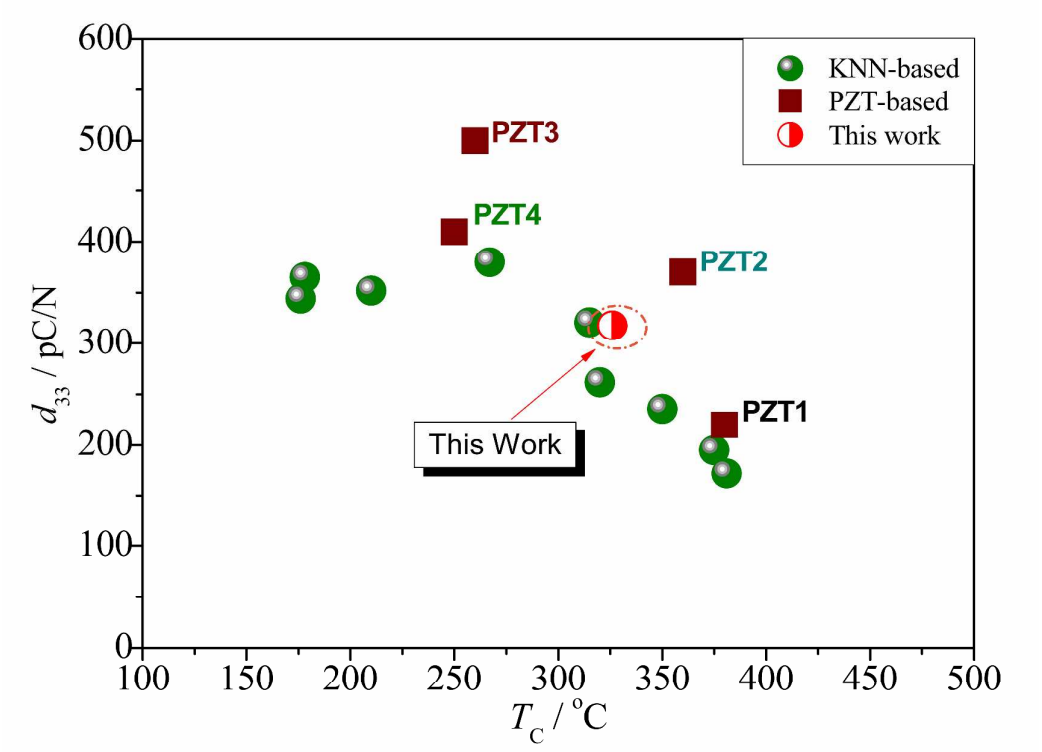

Prime Novelty Statement

The ceramics possess large d_{33} and high T_C, which can mediate the current contradiction of d_{33} and T_C in KNN.